SELF-GRAVITATING TORI AROUND BLACK HOLES AND THEIR INSTABILITIES

NIKOLAOS STERGIOULAS

DEPARTMENT OF PHYSICS
ARISTOTLE UNIVERSITY OF THESSALONIKI

Warsaw, Feb. 22, 2013

Plan of Talk

Motivation

- Equilibrium models of self-gravitating tori around black holes
- Non-axisymmetric instabilities
- Runaway instability
- Prospects

Collaborators:

O. Korobkin (Stockholm), E. Abdikamalov (Caltech),
E. Schnetter (Perimeter Institute), B. Zink (Tuebingen)
S. Rosswog (Stockholm), C. Ott (Caltech)

Publications:

1) Stergioulas, *IJMPD* (2011)
2) Stergioulas, *JPCS* (2011)
3) Korobkin, Abdikamalov, Schnetter, Stergioulas, Zink, *PRD* (2011)
4) Korobkin, Abdikamalov, Schnetter, Stergioulas, Zink, Rosswog, Ott, *MNRAS Letter* (2013)
5) Mewes, Montero, Stergioulas, Galeazzi, Font, *ASSP* (2015)

Importance of Tori for GRBs

Long GRBs

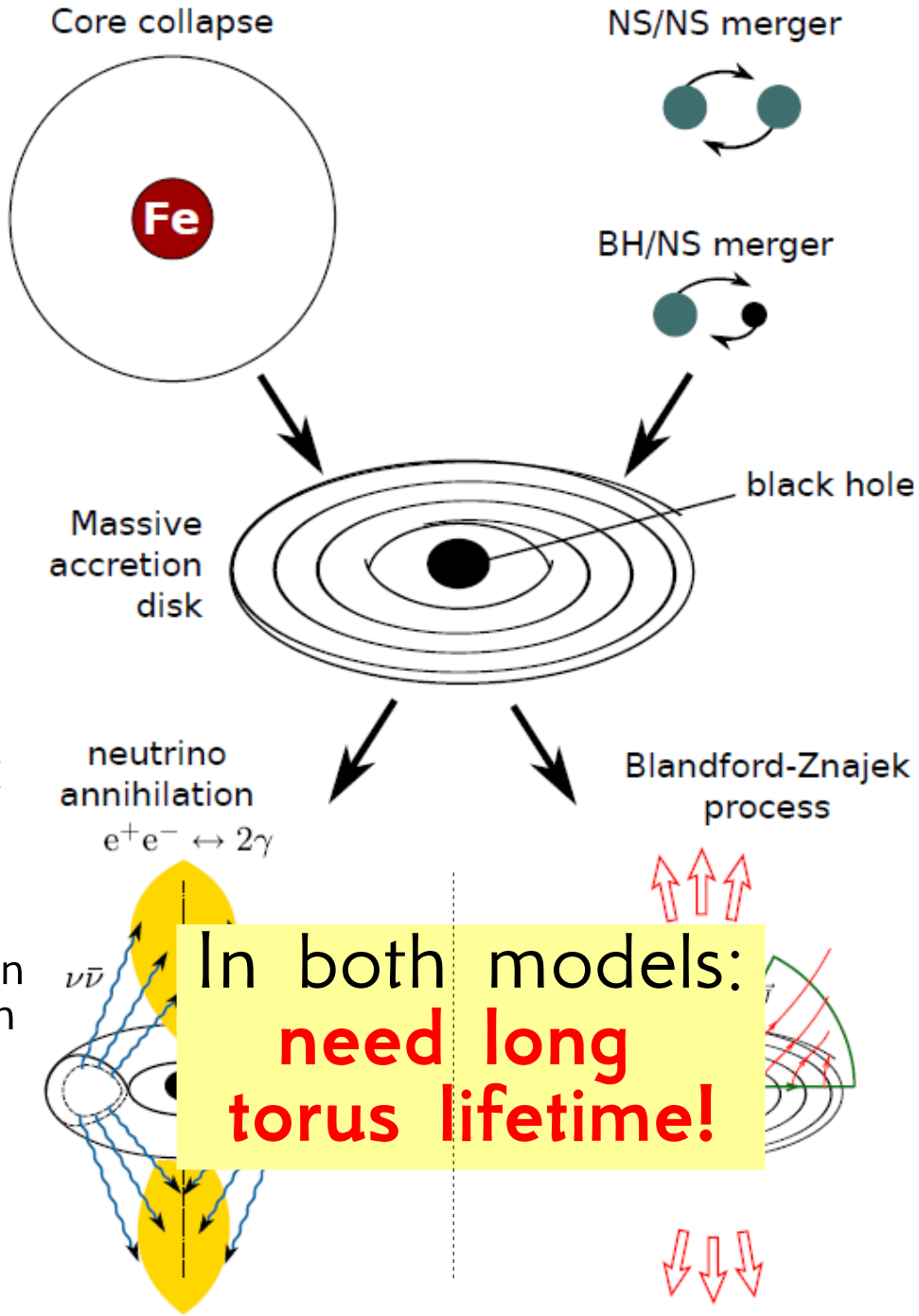

Short GRBs

Torus with mass
~0.01 – 0.2 M_{BH}

Accretion-powered:

hyperaccretion rates
neutrino cooling
neutrino pair annihilation
electron pair annihilation
γ-ray emission

→ GRB

In both models: need long torus lifetime!

BH rotation powered:

strong E/M fields
particle acceleration
γ-ray emission

→ GRB

Neglecting Self-gravity

Abramowicz, Jaroszynski, Sikora (1978)

AJS disks: analytic solutions with simple rotational profile of *constant specific angular momentum* l=const. in a given Kerr background metric.

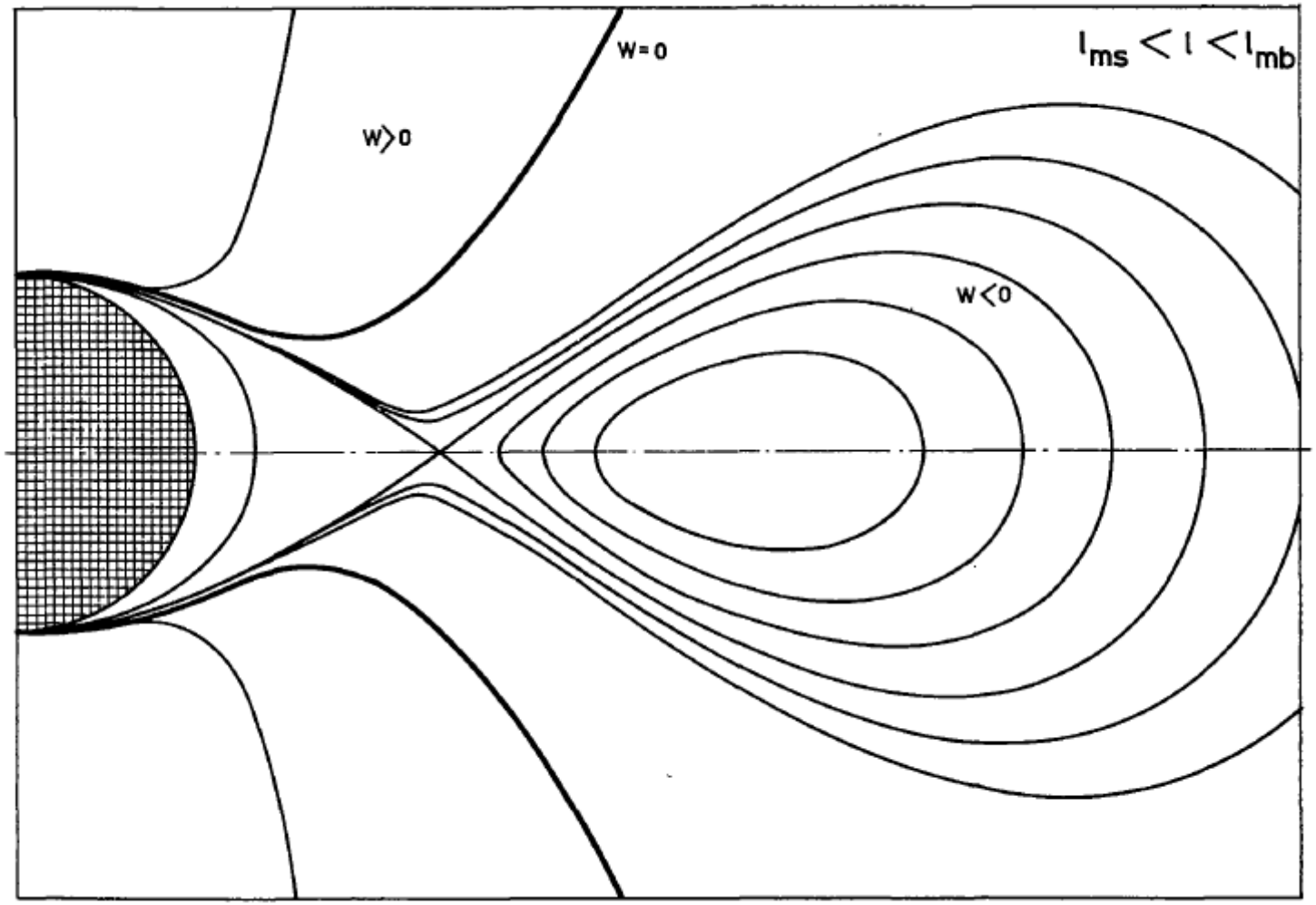

Axisymmetric Runaway Instability

(Abramowicz, Calvani, Nobili, 1983)

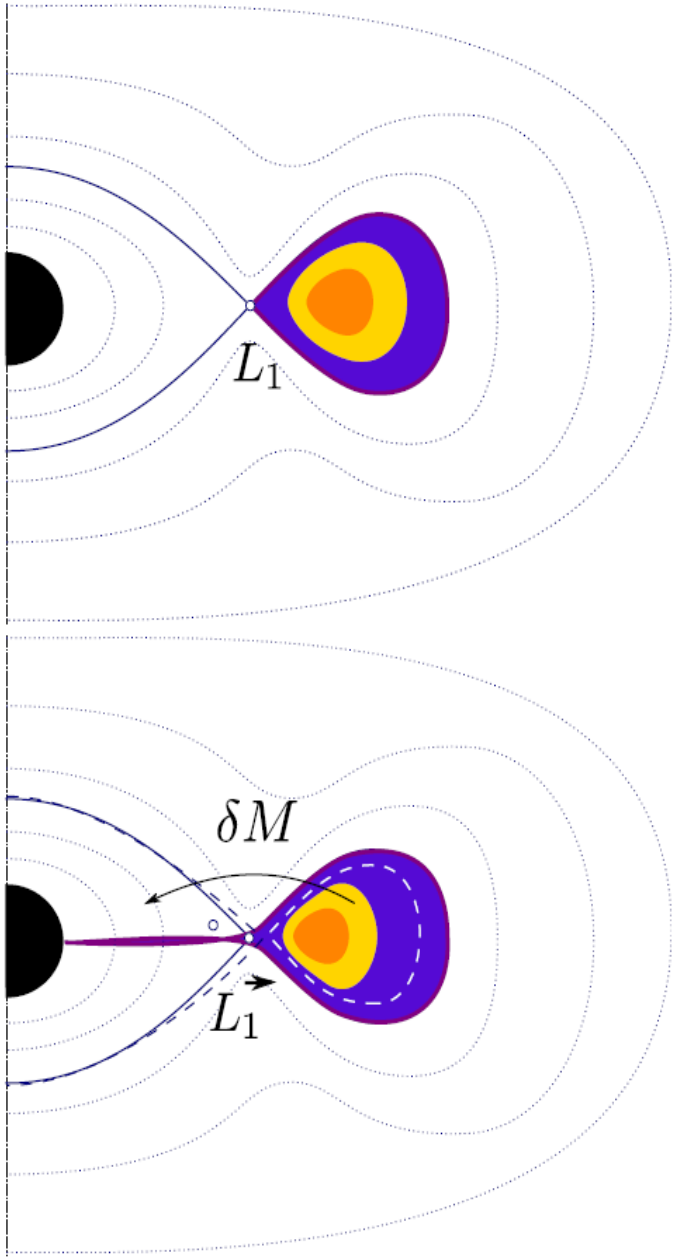

Onset of instability depends on several factors:

Stabilizing factors:

Rotation law (different from l=const.)

Large black hole angular momentum

Destabilizing factors:

LS EOS vs. N=3 Polytrope

Self-gravity

Nonaxisymmetric Instabilities

Without self-gravity (Papaloizou-Pringle 1984) :

P- modes due to *corotation resonance* near the pressure maximum
- becomes weaker as self-gravity increases
- needs a certain range of rotational profiles.

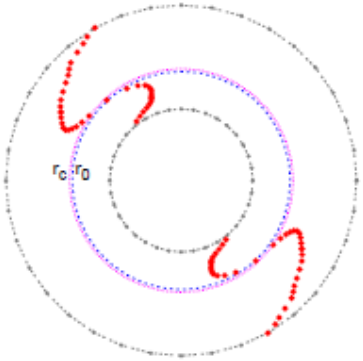

With self-gravity: (Goodman & Narayan 1988)

I- modes: elliptic or other deformations
- need *moderate degrees of self-gravity*

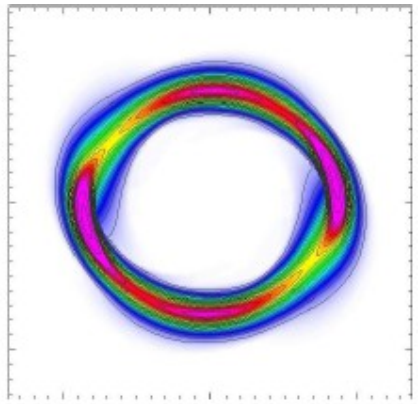

J- modes: essentially the *Jeans instability* when self-gravity is dominant.

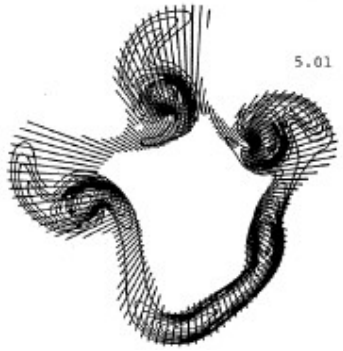

Self-consistent Equilibrium Models

Assuming a stationary and axisymmetric spacetime, the metric can be written as

$$ds^2 = -\lambda^2 dt^2 + e^{2\alpha}\left(dr^2 + r^2 d\theta^2\right) + \left(B\lambda^{-1}\right)^2 r^2 \sin^2\theta \left(d\varphi - \omega\, dt\right)^2$$

with boundary conditions on the horizon: $B = 0,\ \ \lambda = 0,\ \ \omega = \omega_h$

The Euler equation takes the form:

$$\frac{\nabla P}{\epsilon + P} = -\nabla\left(-u_t\right) + \frac{\Omega \nabla l}{1 - \Omega l} = -\nabla W$$

where W is the *effective potential*, l is the specific angular momentum and Ω is angular velocity.

Field Equations

The field equations for 3 of the 4 metric functions can be written as elliptic-type equations:

$$\nabla^2 \lambda = S_\lambda(s,\mu)$$

$$\left(\nabla^2 + \frac{(1-s)^3}{r_e^2 s}\frac{\partial}{\partial s} - \frac{(1-s)^2}{r_e^2 s^2}\mu\frac{\partial}{\partial_\mu}\right) B = S_B(s,\mu)$$

$$\left(\nabla^2 + \frac{2(1-s)^3}{r_e^2 s}\frac{\partial}{\partial s} - \frac{2(1-s)^2}{r_e^2 s^2}\mu\frac{\partial}{\partial_\mu}\right) \omega = S_\omega(s,\mu)$$

(the equation for α is an ODE).

Numerical method: iterative method using Green's functions (Nishida & Eriguchi, 1994)

Here: *radial grid compactification* to the range [0,1]

$$r = r_e \frac{s}{1-s}$$

Equilibrium Properties

Spacetime:

$$M = M_{\mathrm{ADM}} = \lim_{s \to 1} r_e s^2 \frac{\partial \lambda}{\partial s}$$

$$J = J_{\mathrm{K}} = \lim_{s \to 1} -\frac{1}{6} r_e^3 \frac{s^4}{(1-s)^2} \frac{\partial \omega}{\partial s}$$

Black hole:

$$M_{\mathrm{BH}} = C_{\mathrm{eq}} / 4\pi$$

Torus:

$$M_0 = \int \rho u^t \sqrt{-g}\, d^3x$$

$$U_{\mathrm{T}} = \int (\epsilon - \rho) u^t \sqrt{-g}\, d^3x$$

$$J_{\mathrm{T}} = \int T^t{}_{\varphi} \sqrt{-g}\, d^3x$$

$$T_{\mathrm{T}} = \frac{1}{2} \int \Omega T^t{}_{\varphi} \sqrt{-g}\, d^3x$$

$$M_{\mathrm{T}} = \int (-2 T_t{}^t + T_i{}^i) \sqrt{-g}\, d^3x$$

$$W_{\mathrm{T}} = M - M_{BH} - M_0 - T_T - U_T$$

Representative Model

NS (2011)

Table 1. Properties of a representative self-consistent model of a BH-torus system, with $N = 3$, $l/M_{\rm BH}$=3.911, $r_{\rm out}/h_0$=49.005, $\omega_h = 0$ and $K/M_{\rm BH}^{2/N}$=17.339. All radii are coordinate radii in the quasi-isotropic metric.

Asymptotic spacetime mass	$M/M_{\rm BH}$	1.1730
Torus mass	$M_{\rm T}/M_{\rm BH}$	0.2097
Maximum density	$\rho_{\rm max} M_{\rm BH}^2$	6.6126×10^{-5}
Inner torus radius	$r_{\rm in}/M_{\rm BH}$	3.0413
Radius of maximum density	$r_{\rm max}/M_{\rm BH}$	8.1931
Outer torus radius	$r_{\rm out}/M_{\rm BH}$	23.6400
Torus rest mass	$M_0/M_{\rm BH}$	0.1964
Torus internal energy	$U_{\rm T}/M_{\rm BH}$	2.9878×10^{-3}
Torus rotational energy	$T_{\rm T}/M_{\rm BH}$	9.5559×10^{-3}
Torus gravitational potential energy	$W_{\rm T}/M_{\rm BH}$	-3.5865×10^{-2}
Torus rotational to potential energy	$\lvert T/W\rvert_{\rm T}$	0.2664
Torus angular momentum	$J_{\rm T}/M_{\rm BH}^2$	0.7390
Black hole horizon radius	$h_0/M_{\rm BH}$	0.4824
Black hole Komar charge	$M_{\rm H}/M_{\rm BH}$	0.9633

Effective Potential

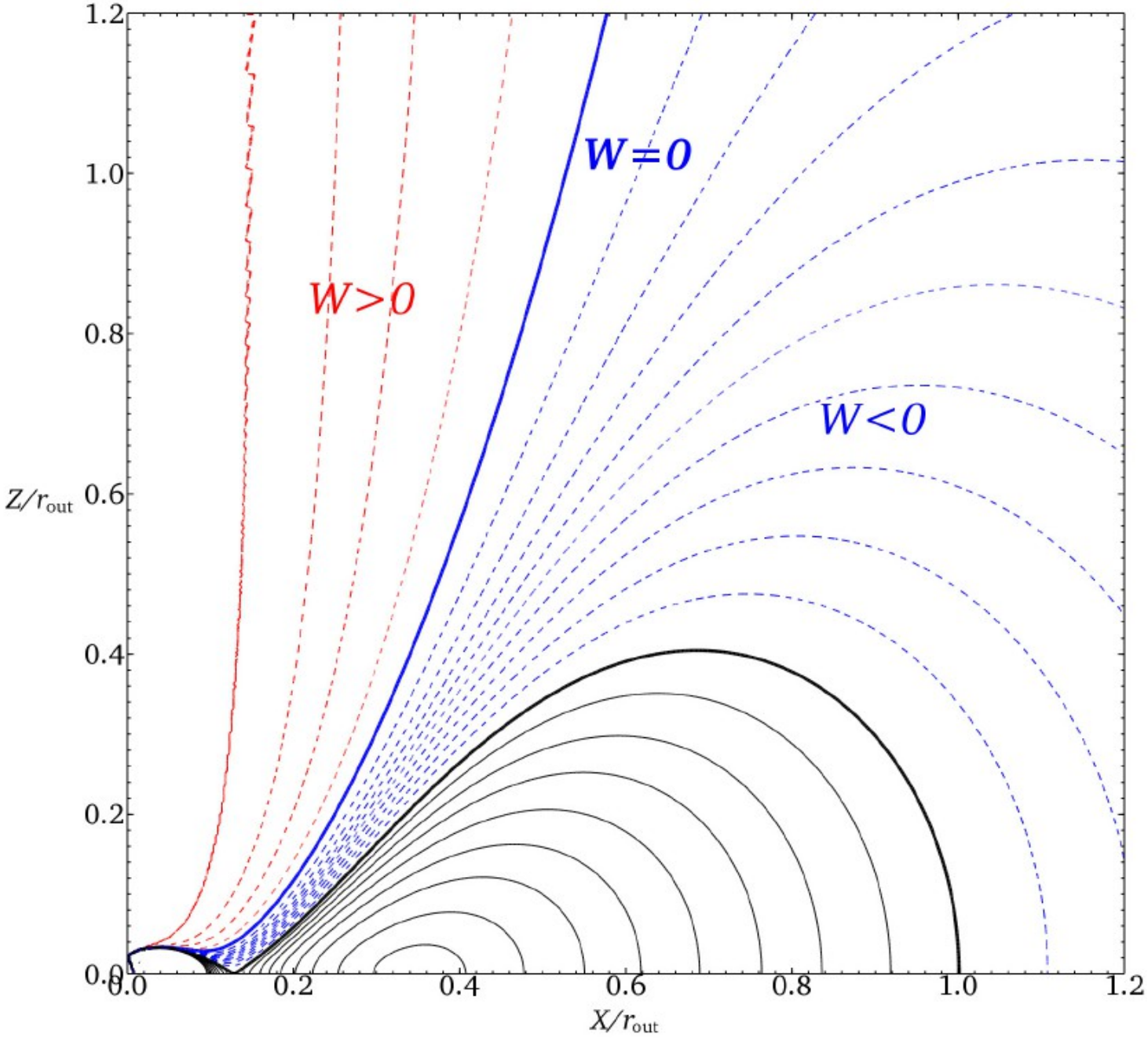

Metric Functions

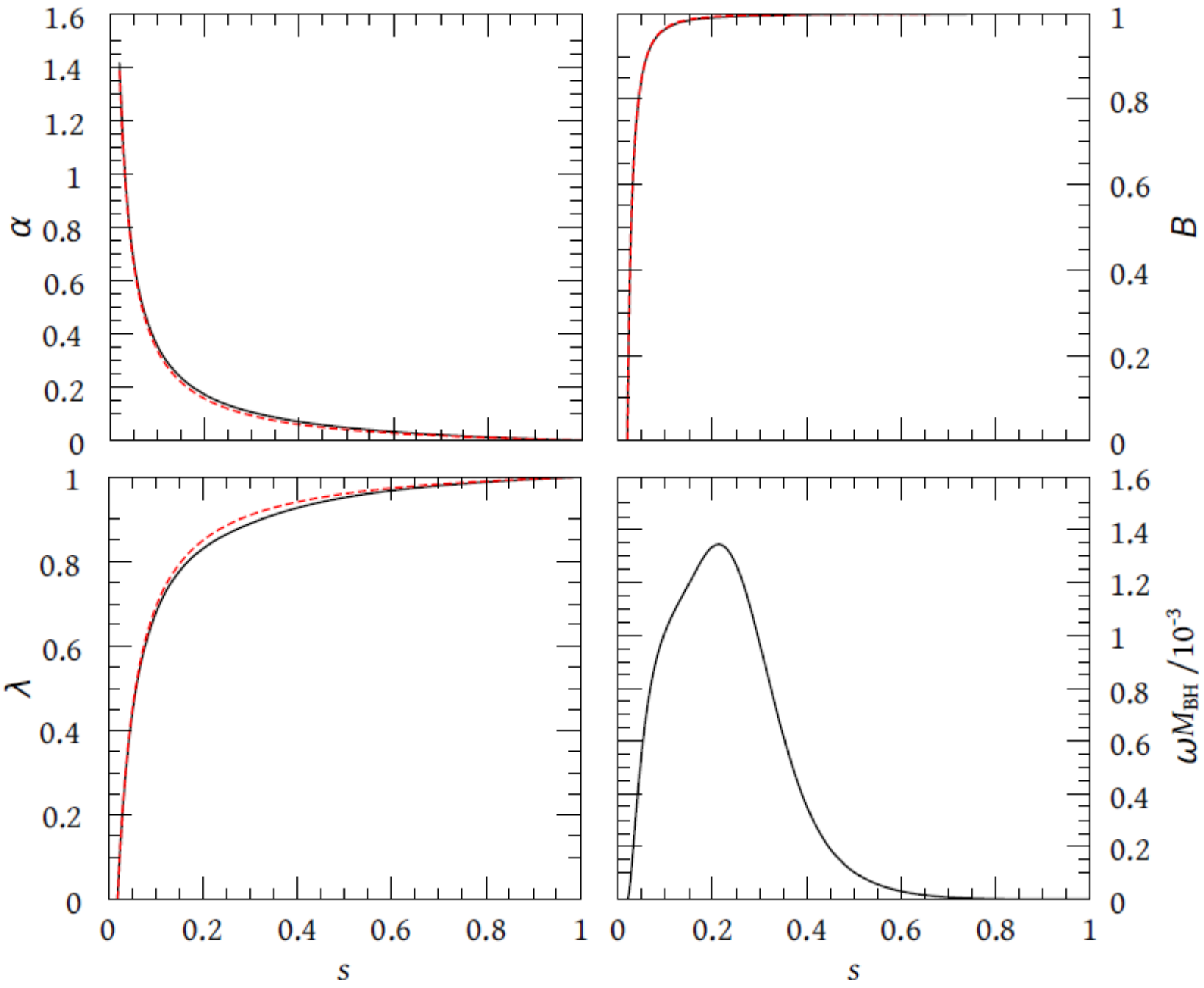

Sequence of Models with Cusp

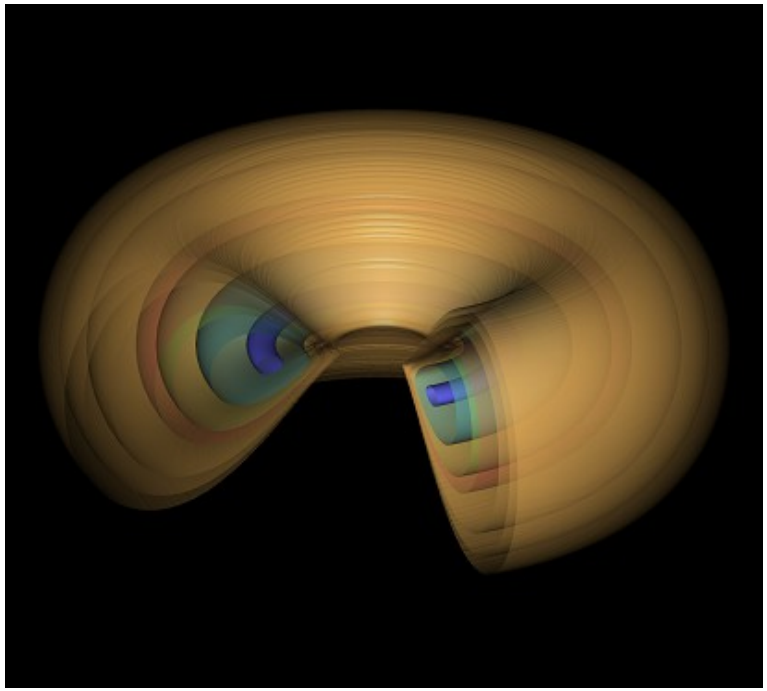

Table 2. Properties of a sequence of models with a cusp with $N = 3$, $l/M_{\rm BH}^{\rm AJS}$=3.675 and $\omega_h = 0$.

$M_{\rm T}/M_{\rm BH}$	$M/M_{\rm BH}$	$l/M_{\rm BH}$	$r_{\rm in}/M_{\rm BH}$	$r_{\rm max}/M_{\rm BH}$	$r_{\rm out}/M_{\rm BH}$	$J_{\rm T}/M_{\rm BH}^2$
–	1.000	3.675	4.838	5.092	5.244	–
0.134	1.107	3.859	3.193	7.763	18.235	0.460
0.296	1.249	3.948	2.888	8.765	39.329	1.079
0.366	1.312	3.952	2.784	9.025	58.745	1.357
0.438	1.379	3.947	2.723	9.167	85.049	1.644
0.546	1.484	3.948	2.660	9.293	133.360	2.074

Sequence of Models with Cusp

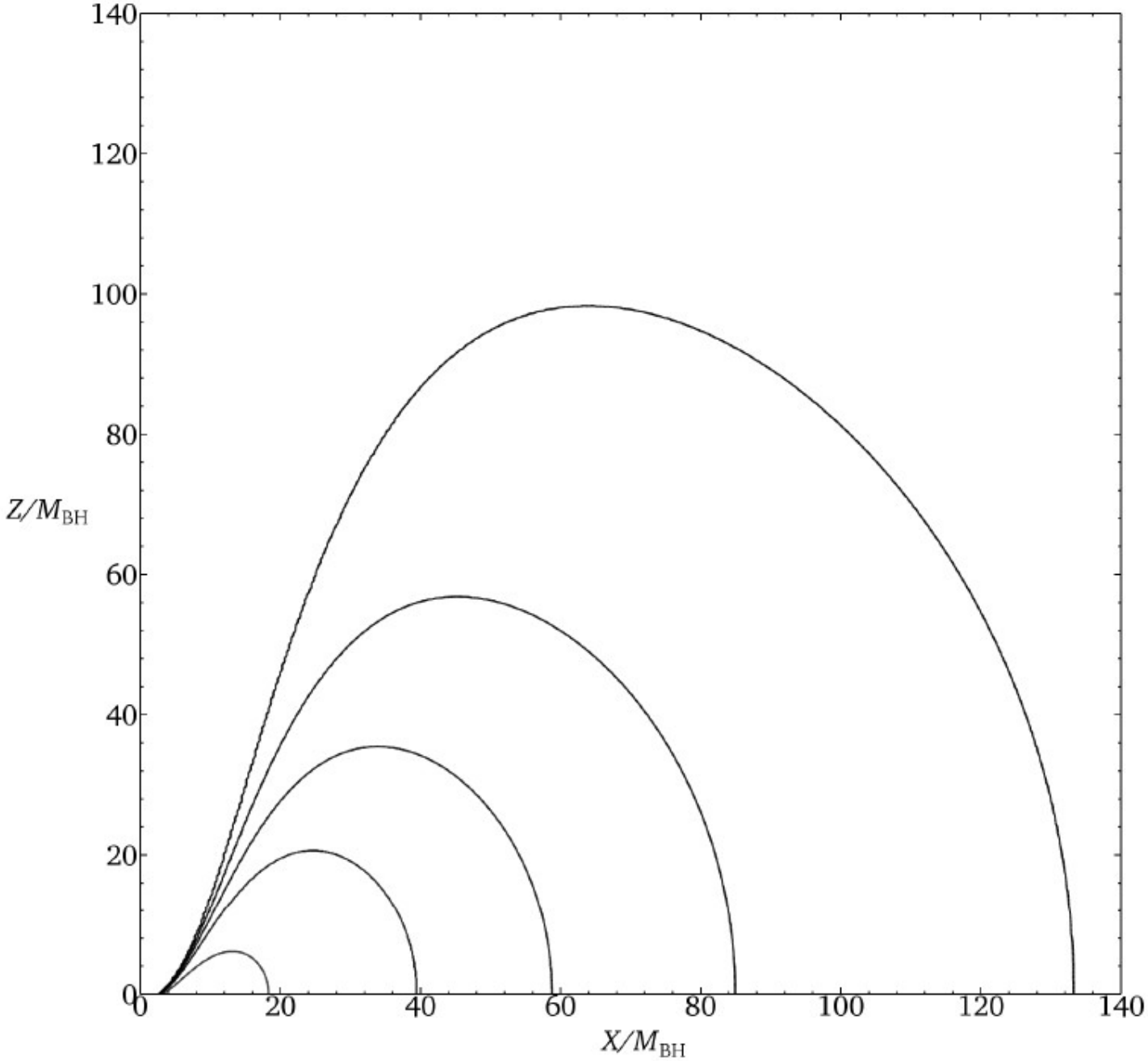

Effective Potential

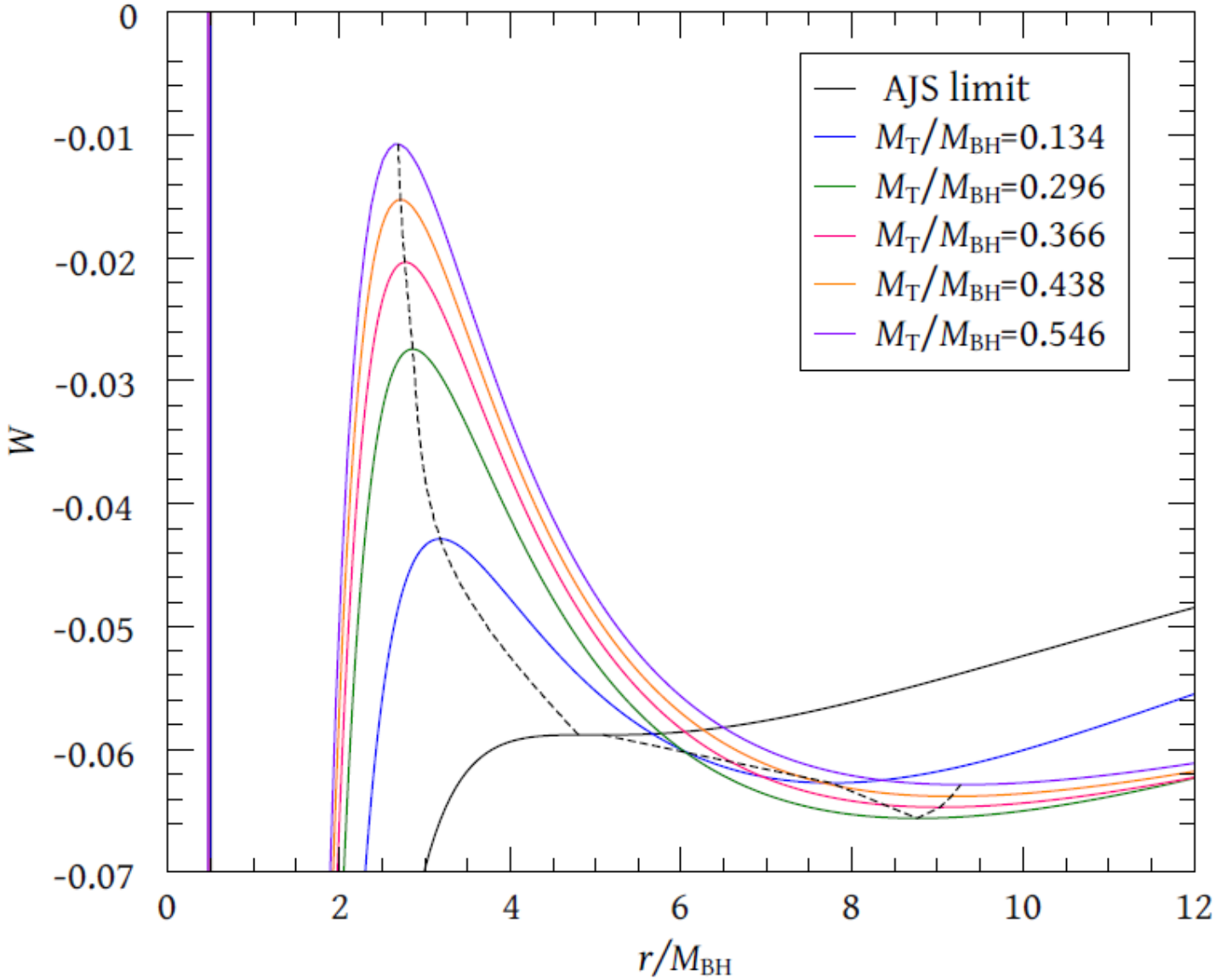

Models with cusp are still limited by $l<4M_{BH}$, as in the case when self-gravity is neglected.

3D Multi-block CACTUS/CARPET Code

Hydrodynamics equations

- Cell-centered finite volumes scheme
- Interpolated boundary conditions
- High-order reconstruction method: PPM
- Riemann solver: HLLE
- Code: THOR*

* [*B. Zink, E. Schnetter, M. Tiglio*, **PRD**, 2008]

Spacetime equations

- Generalized Harmonic formulation*
- Constraint damping mechanism
- High-order dissipative FD operators**
- Multi-block domain, penalty boundary conditions***
- Code: QUILT

* [*L. Lindblom, M. Scheel, L. Kidder, R. Owen, O. Rinne*, **CQG**, 2006]

** [*P. Diener, N. Dorband, E. Schnetter, M. Tiglio*, **J.Sci.Comp.**, 2007]

*** [*L. Lehner, O. Reula, M. Tiglio*, **CQG**, 2005]

Numerical Grid and Initial Data

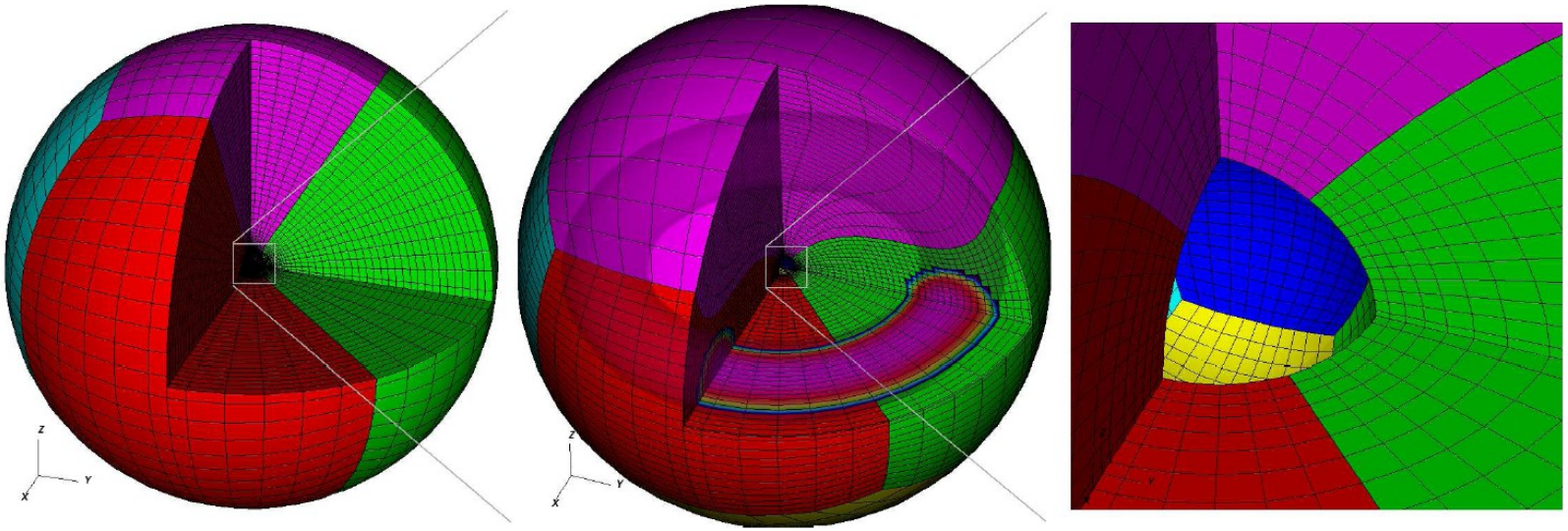

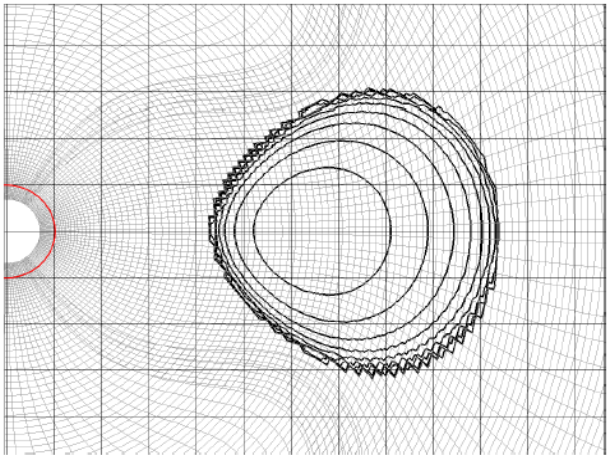

Model A

$M_{\rm A} = 0.24\, M_{\rm BH}$

(massive)

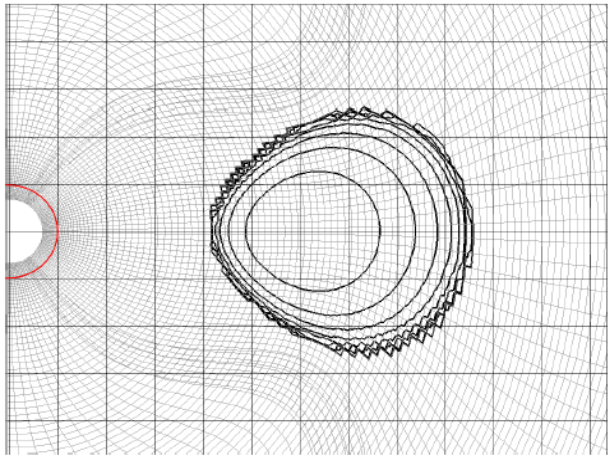

Model B

$M_{\rm B} = 0.17\, M_{\rm BH}$

(mod. slender)

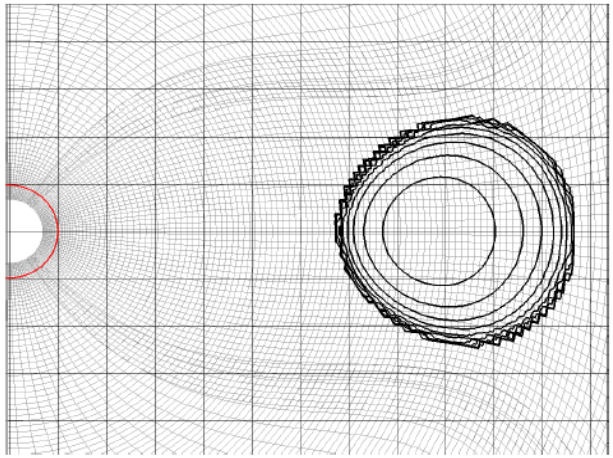

Model C

$M_{\rm C} = 0.11\, M_{\rm BH}$

(slender)

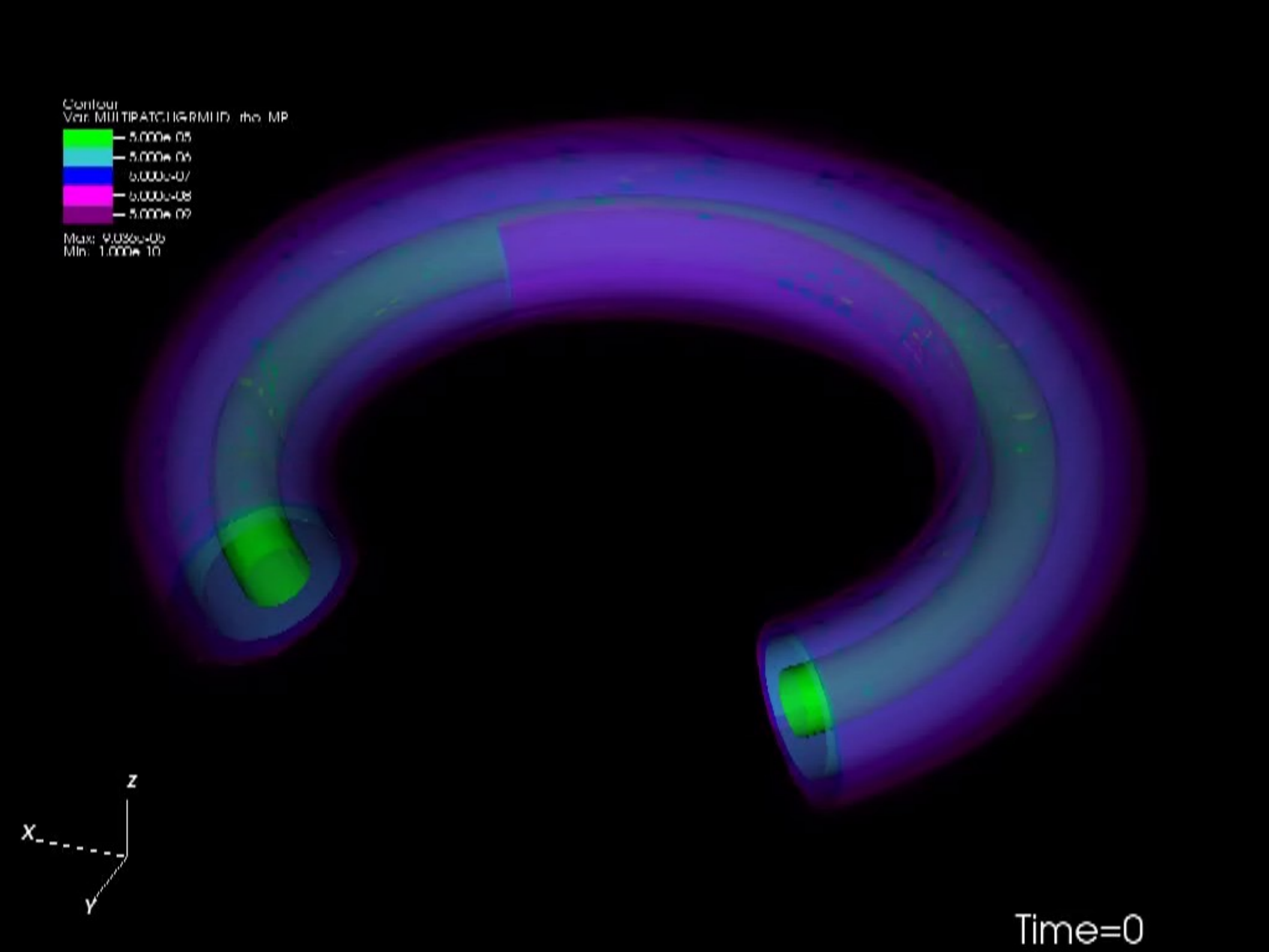
Contour
Var: MULTIPATCHGRMHD rho MP
5.000e 05
5.000e 05
5.000e-07
5.000e-08
5.000e 09
Max: 9.036e-05
Min: 1.000e 10
z
x
y
Time=0

Mode Analysis

Different modes are extracted by Fourier-analyzing the density evolution at concentric rings in the equatorial plane

$$\rho(t, r, \varphi) = \bar{\rho}(t, r)\left(1 + \sum_{m=1}^{\infty} D_m e^{-i(\omega_m t - m\varphi)}\right)$$

From slope of $\varphi_m(t)$ vs. t, extract parameter

$$y_1(m) = \frac{\mathrm{Re}(\omega_m)}{\Omega_{\mathrm{orb}}} - m$$

which yields the *mode pattern speed*

$$\Omega_p = \Omega_{\mathrm{orb}}\left(1 + \frac{y_1(m)}{m}\right)$$

From slope of $ln|D_m|$ vs. t, extract *growth rate parameter*:

$$y_2(m) = \frac{\mathrm{Im}(\omega_m)}{\Omega_{\mathrm{orb}}}$$

Model A: m=1 Papaloizou-Pringle Instability

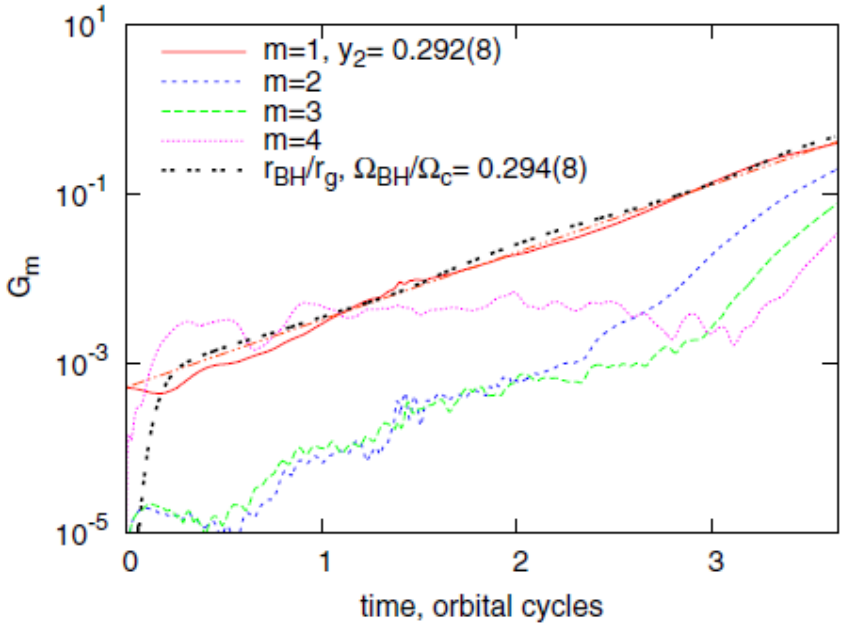

(a)

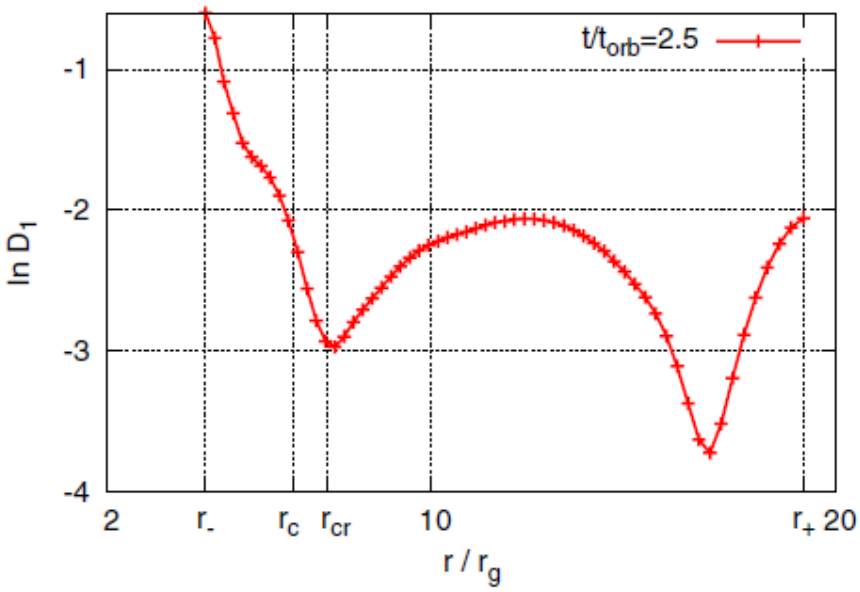

(b)

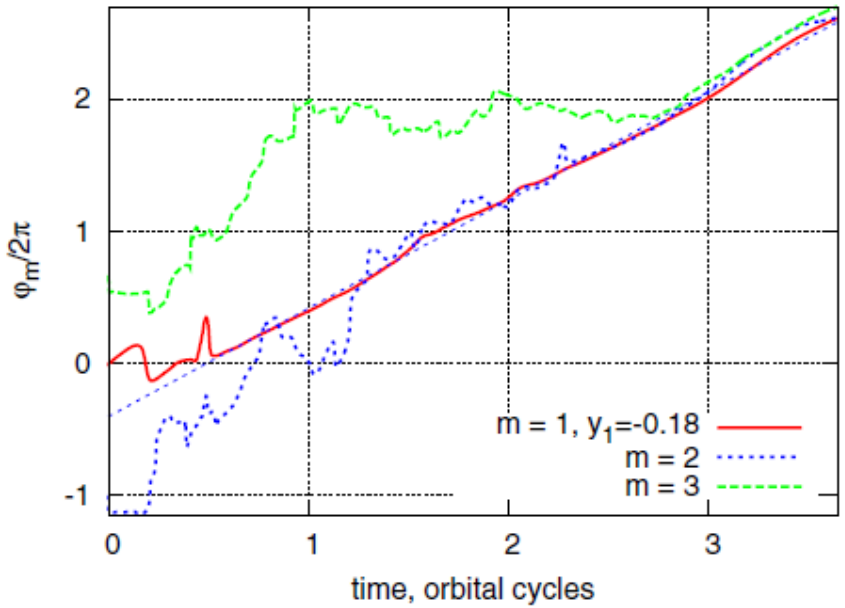

(c)

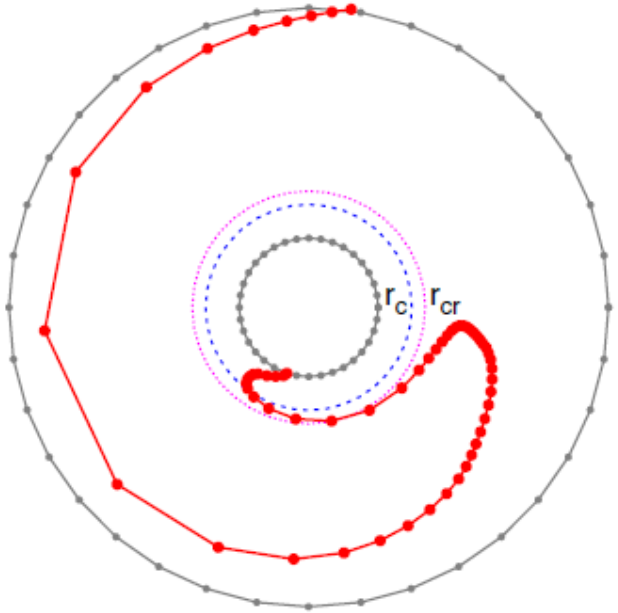

(d)

Model A: m=2 Intermediate Instability

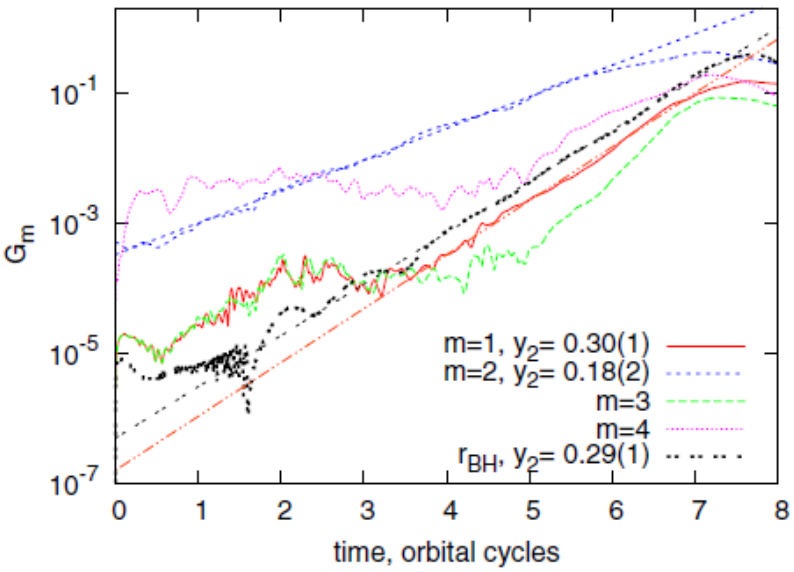

(a)

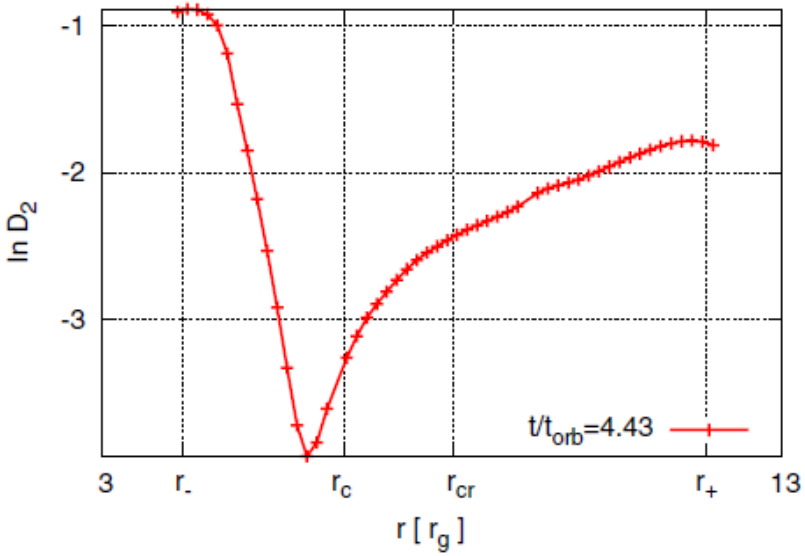

(b)

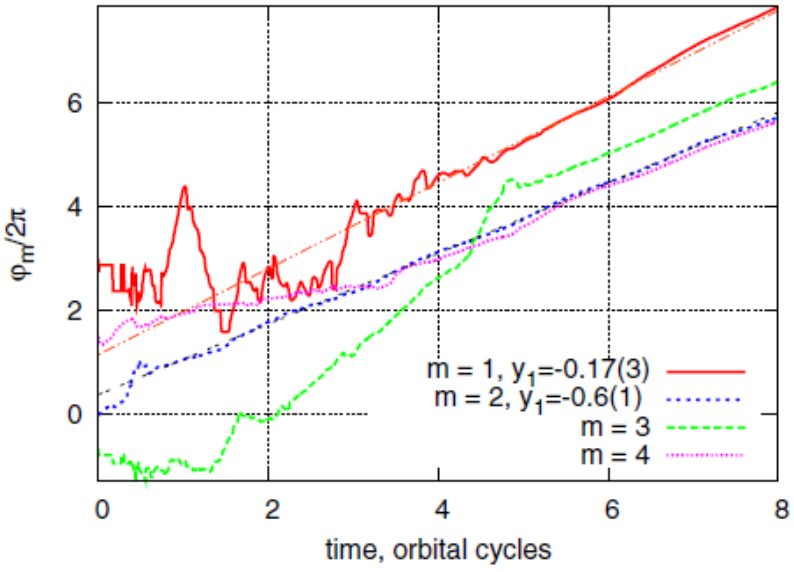

(c)

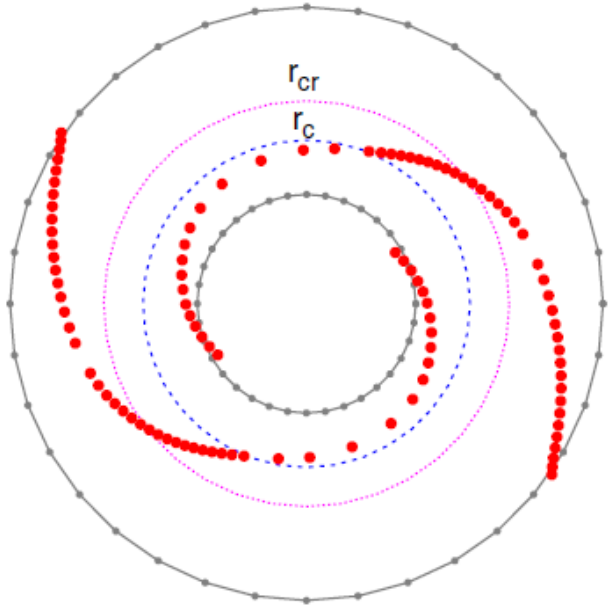

(d)

m=1: Spiral Motion of the BH

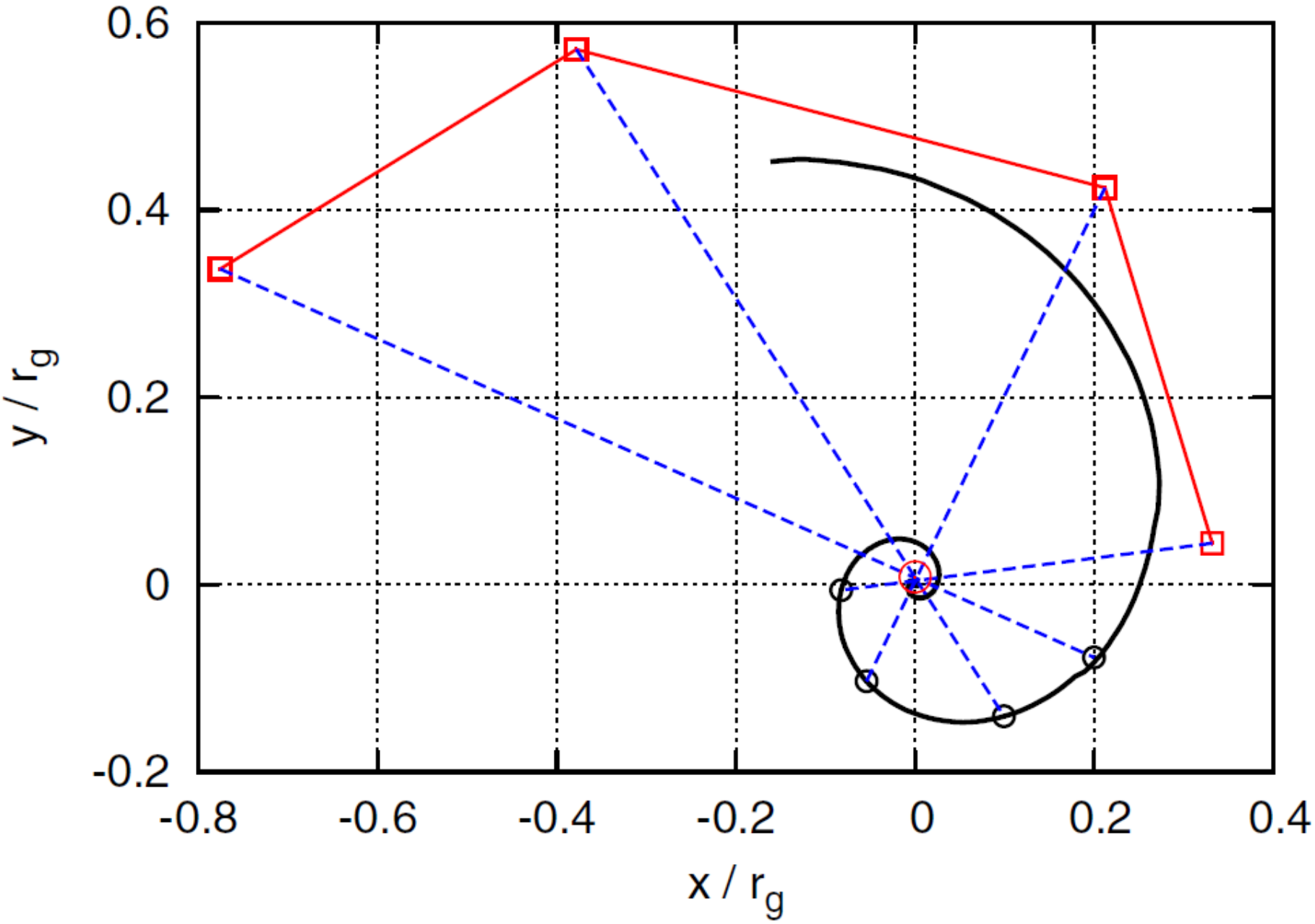

Additional Models

Model A: m=1 PP-mode

m=2 I-mode

Model B: m=1 PP-mode

m=2 I-mode

Model C: m=1 PP-mode

m=2, 3, 4 I-mode

Detectability of GWs

Source	LIGO	Adv. LIGO	ET
Disk A at 10 kpc	~ 2 ms	~ 2 ms	~ 2 ms
Disk C at 10 kpc	~ 5 ms	~ 2 ms	~ 2 ms
Disk A at 18 Mpc	~ 3000 s	~ 14 s	~ 72 ms
Disk C at 18 Mpc	~ 11500 s	~ 140 s	~ 0.3 s

Table: Minimal lifetime for the $m = 2$ instability with amplitude $D_m > 0.1$ needed for detection

(see also Kenta, Shibata, Montero, Font, 2011 for GWs from m=1 PP instability)

Runaway Instability

	model	l=const?	BH rotation	SG	stable?
Abramowicz et al. 1983	PN	yes	no	≈	no
Wilson 1984	GR	yes	yes	no	yes
Khanna, Chakrabarti 1992	PN	yes	yes	≈	no
Nishida et al. 1996	GR	yes	yes	yes	no
Daigne, Mochkovitch 1997	PN	no	no	no	yes
Abramowicz et al. 1998	GR	no	yes	no	yes
Masuda et al. 1998	PN	no	no	yes	no
Lu et al. 2000	PN	no	no	no	yes
Font, Daigne 2002*	GR	yes	no	no	no
Zanotti et al. 2003	GR	yes	no	no	no
Daigne, Font 2004	GR	no	no	no	yes
Montero et al. 2010	FGR	yes	no	yes	yes
Rezzolla et al. 2010	FGR	no	yes	yes	yes

* Table adopted from *Font J. A., Daigne F.*, 2002, **MNRAS**

Simulations

fixed spacetime, 2D

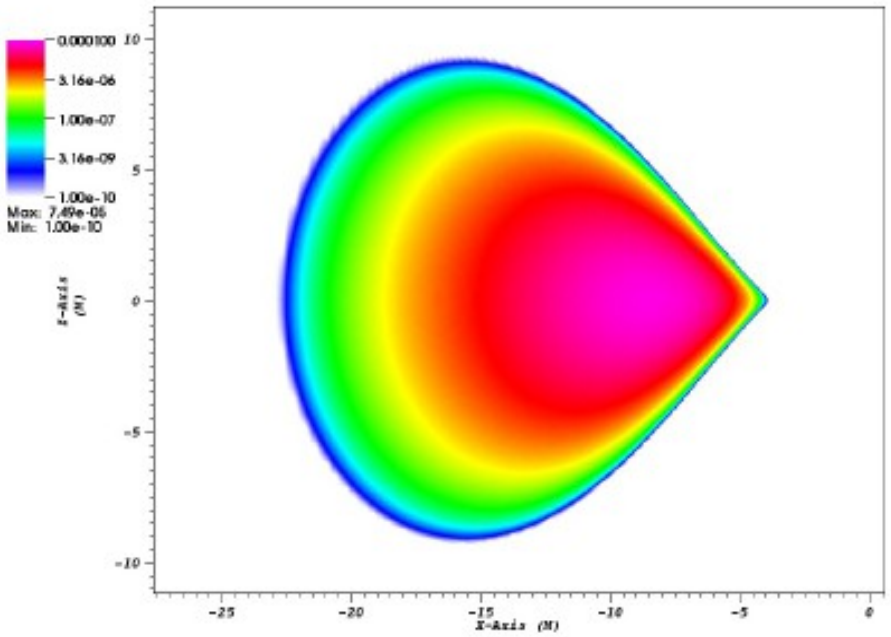

Time=0

dynamical spacetime, 3D

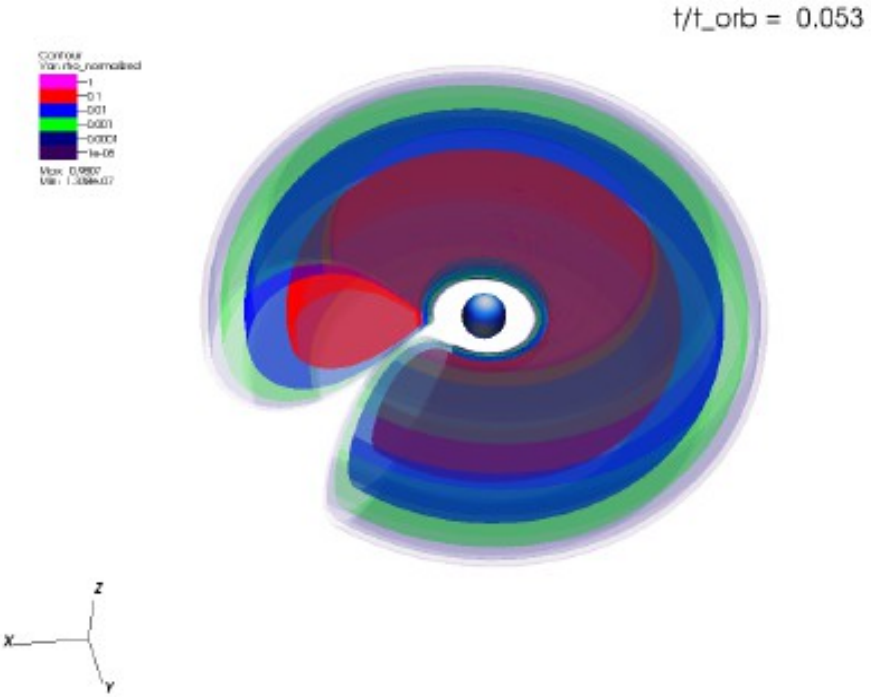

Runaway Instability

Mass of the BH

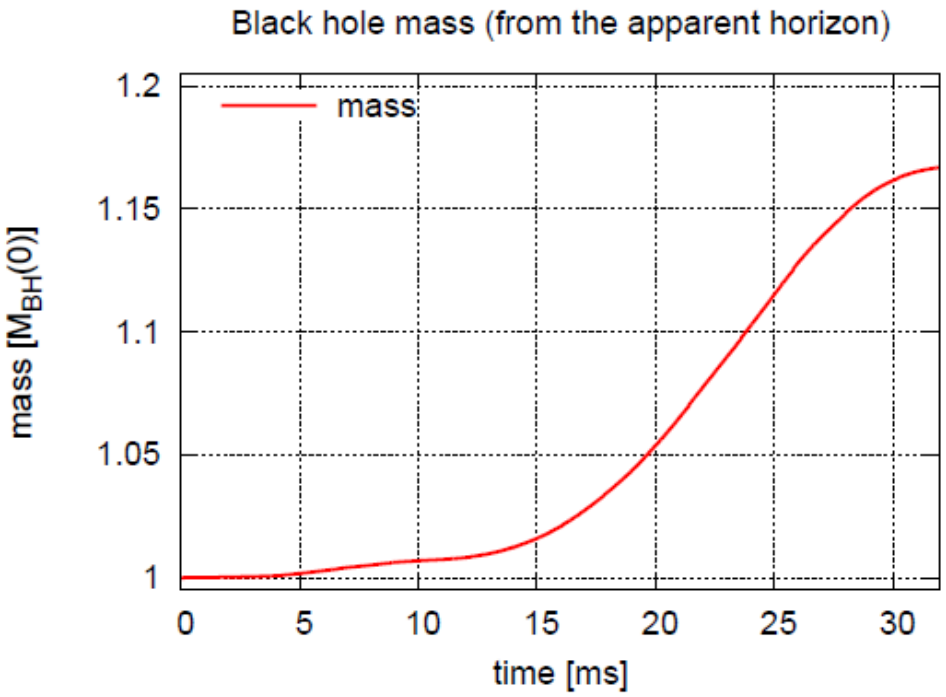

Mass of the disk

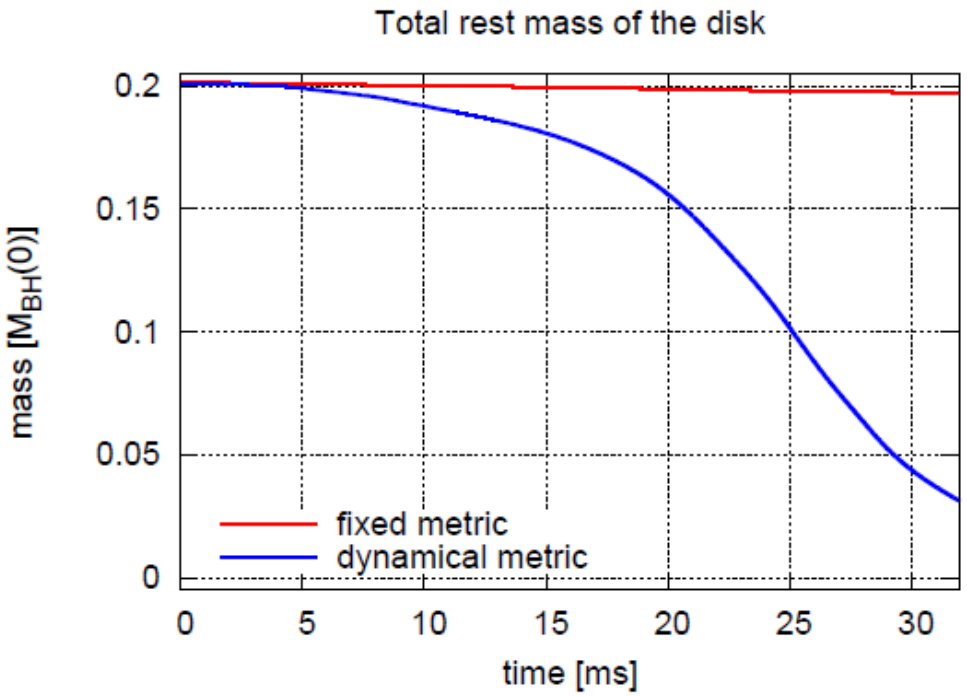

Runaway Instability

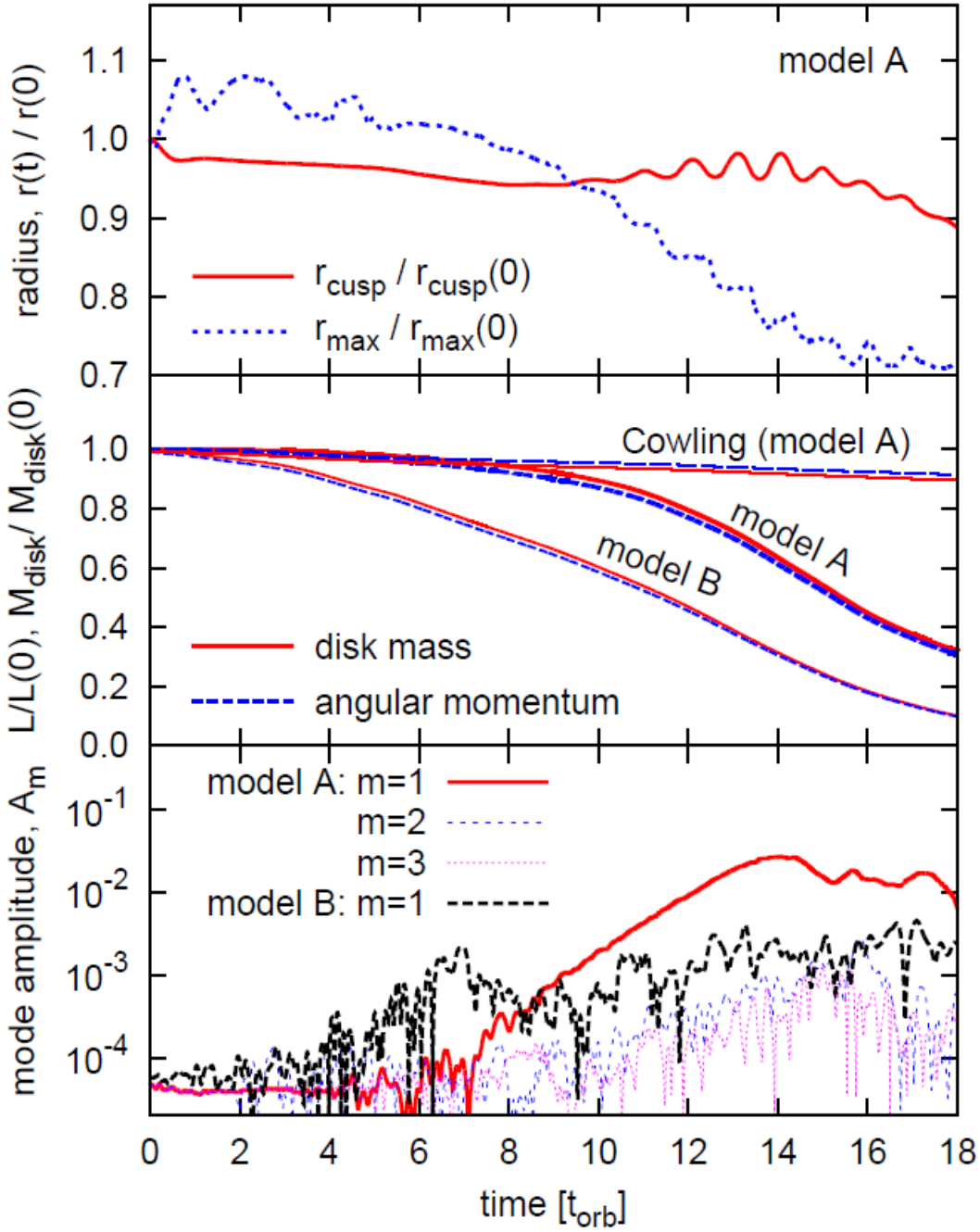

Conclusions

Nonaxisymmetric instabilities

- All models exhibit nonaxisymmetric instabilities.
- Unstable m=1 modes are PP-modes.
- Unstable m>1 modes are I-modes.
- Potential source of GWs.

Runaway instability

- It exists also in full GR, at least under the most favourable condition of l=const.

Prospects:

- Investigate the role of nonaxisymmetric instabilities in nonlinear saturation of the runaway instability.
- Investigate tilted accretion disks (in preparation).